

# A fast topology optimisation for material- and geometry-independent cloaking devices with the BEM and the $\mathcal{H}$ -matrix method

Kenta Nakamoto<sup>1</sup>, Hiroshi Isakari<sup>1</sup>, Toru Takahashi<sup>1</sup>, and Toshiro Matsumoto<sup>1</sup>  
 1. Nagoya University, Japan

**Abstract:** We show a design method of cloaking devices which work for target objects with arbitrary shape and material by a topology optimisation with an accurate and efficient sensitivity analysis. Most of past researches on topology optimisation of cloaking devices intend to hide a circle-shaped perfect electric conductor. In this case, the cloaking effect is highly dependent on the shape and material of a target object. In this study, we consider to design a cloaking device which work regardless of the property of target objects by modifying the definition of the objective function. Also, we developed an efficient and accurate sensitivity analysis with the boundary element method and the  $\mathcal{H}$ -matrix method. We show that the proposed method can successfully obtain desired cloaking devices with low computational cost.

## 1. INTRODUCTION

Establishment of the theory to control the electro-magnetic field with metamaterials [1] has encouraged developments of innovative optical devices such as metamaterial-based waveguides [2] and superlens [3], etc. As one of the most attractive applications of metamaterials, cloaking has extensively been researched so far. The cloaking is a technology to make an object invisible by reducing the scattering around the object. There are two main ways to construct cloaking devices; light pass controlling and scattering cancellation. The former strategy was proposed by Pendry et al [4], in which they theoretically showed the possibility to construct a cloaking device by periodically putting metamaterials whose permeability is negative. By covering a target object with the cloaking device,

the light pass is controlled to go around the target object, which makes the object invisible. Smith et al. experimentally created a cloaking device by allocating metamaterials periodically and showed that their cloaking works to hide a copper cylinder in TM polarised microwave range [5]. While their cloaking device can hide arbitrary-shaped target objects, it is made of anisotropic and inhomogeneous materials which may cause difficulty in manufacturing. Furthermore, their cloaking device has some critical problems from an engineering standpoint. Their cloaking may cause an energy loss and works only when the frequency of the incident field is in a narrow target range. As the latter type of cloaking, Alú and Engheta proposed to reduce scattering from spherical and cylindrical objects by covering them with properly designed epsilon-near-zero (ENZ) material [6] which is a kind of metamaterials whose real part of macroscopic permittivity is close to zero. By the use of the ENZ material as a cover, we can suppress the dipolar term in the Mie expansion of the scattered field from a plane wave. Their cloaking device can be made of low loss isotropic and homogeneous material and works in a wide bandwidth. Many researches on cloaking based on scattering cancellation with ENZ material are reported [7, 8]. These cloaking devices, however, need to be designed carefully in accordance with the shape of the target object. When the shape of the target object is perturbed from the expected one, the cloaking may not work. One can find that both methods have some pros and cons, and it is important to develop a design method which is loss less, wide band, easily fabricated and robust to change of shape of target object.

Recently, simulation-based design methods for engineering devices have been applied to many varieties of fields. Topology optimisation has extensively been researched as one of such design methods. Compared with the other methods such as shape optimisation, topology optimisation is the most flexible design method since we can determine not only peripheral shape but also topology of devices. The first pioneering research on an application of the topology optimisation for engineering devices was conducted by Bendsoe and Kikuchi in a design problem of elastic member to maximise its stiffness [9]. They proposed to express structure of devices as distribution of a characteristic function and determine the optimal distribution of the characteristic function which minimises the compliance (work by external force) by iterative update of the material distribution based on a sensitivity analysis. The topology optimisation, however, suffered from numerical instability such as mesh-dependency of optimal configurations or checkerboard patterns. To avoid these problems, some relaxation methods such as the density method [10] or the homogenisation method [9] are proposed. Now, the topology optimisations are widely extended to design problems in engineering

fields other than structural mechanics. In the following, we briefly review some contributions related to applications of the topology optimisations to cloaking devices. Andkjær and Sigmund achieved to obtain some symmetric cloak designs with dielectric elements which work for some angles of incidence by using the density-based topology optimisation [11]. Also, Andkjær et al. succeeded in designing a cloaking device that is effective for both transverse electric (TE) and transverse magnetic (TM) polarisations with the density-based topology optimisation [12]. Relaxation methods, however, allows the existence of grayscale; region which has intermediate density between void and material domain, which makes it difficult to fabricate the obtained configuration. With the help of SIMP method [10], the intermediate density can be removed but parameters for the SIMP method are chosen by a trial and error process. With a careless choice of the parameter, the optimality may be lost. As one of the most promising grayscale-free topology optimisations, we can mention the level-set-based topology optimisation [13]. In the level set method, boundary of design object can be expressed clearly as a zero-level contour of a level-set function. Also, by the use of the reaction-diffusion equation for the update of the level-set function, complexity of the design object can easily be adjusted [14, 15].

Many researches on the level-set based topology optimisation of cloaking devices have been reported. Fujii et al. succeeded to design a cloaking device which works in TM polarised field with the level-set based topology optimisation [16]. Otomori et al. designed a cloaking device made of a ferrite material by using the level set-based topology optimisation and succeeded in designing a cloaking device in TM polarised field [17]. Their cloaking devices are, however, designed in a way to hide a circle-shaped PEC and do not work when the shape and/or material of the target objects are perturbed. For engineering applications, it is necessary to design a cloaking device which works stably regardless of the property of target object. One of the most significant contribution of this paper is to propose a new level-set-based topology optimisation for cloaking devices which is robust to the perturbation of target object. To this end, we modify the definition of the objective function in a way to suppress not only scattered field around a cloaking device but also the intensity of electro-magnetic field in a domain where the target objects to be allocated. By this definition, designed cloaking device is expected to work independently on property of target objects.

Also, previous researches on topology optimisation of cloaking devices have a problem with respect to treatment of a design sensitivity. In the topology optimisation, configuration of a design object is updated repeatedly based on a topological derivative; sensitivity of an objective function with respect to creation of an infinitesimal circular-shaped material in a design domain. By the use of the adjoint variable method, the topological derivative is expressed with solutions of two boundary value problems; so called forward and adjoint problem. The performance of the topology optimisation is highly dependent on how accurately and efficiently forward and adjoint problem are solved. In almost all of researches on topology optimisation, the finite element method (FEM) is employed for the sensitivity analysis. In the FEM, however, the infinite domain where the forward and adjoint problem for cloaking design are often defined should be approximated by a large but finite domain with appropriate boundary conditions. Hence, for enough accuracy we need huge analysis domain, which leads large numerical cost to generate a mesh and finite element analysis. In this study, we employ the boundary element method (BEM) instead of the FEM for the sensitivity analysis. In the BEM, mesh generation is required only on the boundary. Also, the infinity itself is treated as a boundary in the BEM and the condition at the infinity can be satisfied strictly with the help of the Green function. Our previous researches have shown the effectiveness of the level-set based topology optimisation with the BEM in the electromagnetic field [18], heat conduction problem [19, 20] and sound field problem [21, 22]. We further improve our previous BEM-based optimisations to develop an efficient computation of the topological derivative. The forward and adjoint problem can be reduced to algebraic equations by a numerical analysis method such as the FEM or BEM. These two equations can be solved efficiently with direct solvers such as the LU decomposition since the coefficient matrices of these equations are the same in many cases. The coefficient matrix derived by the BEM is, however, fully-populated, which causes large numerical cost for generation of the coefficient matrix and the LU decomposition. Hence for the fast computation of the topological derivative, acceleration of the BEM and LU decomposition is necessary. The fast multipole method (FMM) is well known acceleration method for the BEM [23, 24]. The FMM is usually combined with iterative solvers for algebraic equations because it is a method to accelerate the matrix-vector product of the BEM coefficient matrix with an arbitrary vector. Hence, we need to solve the forward and adjoint problem individually. Also, the number of iterations to obtain the solution is highly dependent on the property of problems such as complexity of geometry and material constant. In this

study, as an alternative acceleration method for the BEM, we employ the  $\mathcal{H}$ -matrix method [25, 26] which is based on hierarchical blocking of the coefficient matrix and low rank approximation. This method can easily be combined with direct solvers. Furthermore, we can reduce the cost to generate the coefficient matrix and memory to store the matrix by using the adaptive cross approximation (ACA) for the low rank approximation. Hence, it is expected that we can accelerate the sensitivity analysis by using the efficient computation of the coefficient matrix with the ACA and the accelerated LU decomposition by the  $\mathcal{H}$ -matrix method.

The rest of this paper is organised as follows: In the second section, we formulate the level-set based topology optimisation method for cloaking devices. In the third section, we show the derivation of the topological derivative. In the fourth section, we explain about the electro-magnetic field analysis with the BEM. In the fifth section, we introduce an efficient computation of the topological derivative with the  $\mathcal{H}$ -matrix method. In the sixth section, we show the effectiveness of proposed methods with some numerical examples.

## 2. TOPOLOGY OPTIMISATION OF CLOAKING DEVICES

In this section, we define conventional and proposed optimisation problems to design cloaking devices. We also show the procedure for solving the optimisation problems including configuration expression and its update.

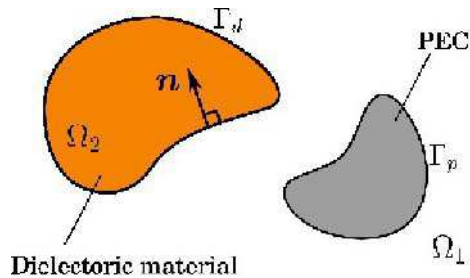


FIGURE 1. Definition of symbols.

### 2.1. A conventional optimisation problem in design for cloaking devices and its modification.

In this study, we consider optimisation problems of cloaking devices in two-dimensional TM polarised field and assume that cloaking device is made of dielectric elements. For the time being, we assume that objects to be hidden is made of perfectly electric conductor (PEC). This restriction will be removed in the proposed optimisation method. We denote a vacuum domain, dielectric elements and PEC as  $\Omega_1$ ,  $\Omega_2$  and  $\Omega_p$ , respectively. Also, we express boundaries of  $\Omega_2$  and  $\Omega_p$  by  $\Gamma_d$ ,  $\Gamma_p$  (Figure 1). Purpose of cloaking devices is to make the PEC invisible by suppressing the scattered field around the PEC. Previous researches have achieved this by determining configuration of cloaking devices which reduce the intensity of scattered

field. In this case, the design problem can be formulated as the following optimisation problem:

$$\begin{aligned}
& \text{Find } \Omega_2 \text{ in } D \\
& \text{such that min } J \\
(1) \quad & J = \sum_{m=1}^M \|u(\mathbf{x}_m^1) - u^{\text{inc}}(\mathbf{x}_m^1)\|^2 \\
(2) \quad & \text{subject to} \\
(3) \quad & \nabla^2 u(\mathbf{x}) + k_1^2 u(\mathbf{x}) = 0 \quad \mathbf{x} \in \Omega_1, \\
(4) \quad & \nabla^2 u(\mathbf{x}) + k_2^2 u(\mathbf{x}) = 0 \quad \mathbf{x} \in \Omega_2, \\
(5) \quad & u^1 = u^2 \quad \mathbf{x} \in \Gamma_d, \\
(6) \quad & \frac{1}{\mu_1} \left( \frac{\partial u}{\partial n} \right)^1 = \frac{1}{\mu_2} \left( \frac{\partial u}{\partial n} \right)^2 \quad \mathbf{x} \in \Gamma_d, \\
(7) \quad & u = 0 \quad \mathbf{x} \in \Gamma_p, \\
(8) \quad & \text{Radiation condition} \quad \mathbf{x} \rightarrow \infty,
\end{aligned}$$

where  $u$  (resp.  $u^{\text{inc}}$ ) denotes the total electric field (resp. incident field), and  $D$  denotes a fixed design domain in which a circle-shaped PEC  $\Omega_p$  is allocated (Figure 2, left). Also,  $\mathbf{x}_m^1$  ( $m = 1, \dots, M$ ) denotes an observation point allocated in an observation domain  $\Omega_{\text{obs}}^1$  around the design domain  $D$ , and  $M$  is the number of the observation points. In the boundary conditions (5) and (6) on  $\Gamma_d$ , the variable with the superscripted index  $i$  denotes the limit of the variable to the boundary  $\Gamma_d$  from  $\Omega_i$ . Also,  $\mu_i$  denotes the permeability of domain  $\Omega_i$ , and  $\partial/\partial n := \mathbf{n} \cdot \nabla$  denotes an outward normal derivative from  $\Omega_1$ .  $k_i$  in equations (3) and (4) is the wave number defined as follows with angular frequency  $\omega$  and permittivity  $\varepsilon_i$  in  $\Omega_i$ :

$$(9) \quad k_i = \omega \sqrt{\mu_i \varepsilon_i}.$$

The optimal configuration of this problem is, however, highly specialised to the circular PEC, and the effectiveness is declined when the PEC is replaced by other shaped one. To avoid this problem, we modify the optimisation problem. We augment the objective function by adding the sum of the intensity of the electric field in a fixed circular domain  $\Omega_{\text{obs}}^2$  which covers the PEC  $\Omega_p$  in the conventional optimisation problem. i.e., the optimisation problem is defined as follows:

$$\begin{aligned}
& \text{Find } \Omega_2 \text{ in } D \\
& \text{such that min } J \\
(10) \quad & J = \sum_{m=1}^M \|u(\mathbf{x}_m^1) - u^{\text{inc}}(\mathbf{x}_m^1)\|^2 + \sum_{n=1}^N \|u(\mathbf{x}_n^2)\|^2 \\
(11) \quad & \text{subject to,} \\
(12) \quad & \nabla^2 u(\mathbf{x}) + k_1^2 u(\mathbf{x}) = 0 \quad \mathbf{x} \in \Omega_1 \cup \Omega_{\text{obs}}^2, \\
(13) \quad & \nabla^2 u(\mathbf{x}) + k_2^2 u(\mathbf{x}) = 0 \quad \mathbf{x} \in \Omega_2, \\
(14) \quad & u^1 = u^2 \quad \mathbf{x} \in \Gamma_d, \\
(15) \quad & \frac{1}{\mu_1} \left( \frac{\partial u}{\partial n} \right)^1 = \frac{1}{\mu_2} \left( \frac{\partial u}{\partial n} \right)^2 \quad \mathbf{x} \in \Gamma_d, \\
(16) \quad & \text{Radiation condition} \quad \mathbf{x} \rightarrow \infty,
\end{aligned}$$

where  $\mathbf{x}_n^2$  ( $n = 1, \dots, N$ ) denotes an observation point in  $\Omega_{\text{obs}}^2$ , and  $N$  is the number of observation points. By the above definition, it is expected to obtain the cloaking device which works regardless of the PEC shape since scattering on the surface of PEC allocated in  $\Omega_{\text{obs}}^1$  will be almost zero. Furthermore, it is expected that the obtained cloaking device work even when the PEC is replaced by dielectric one.

In the following subsections, a procedure to solve the optimisation problems is presented.

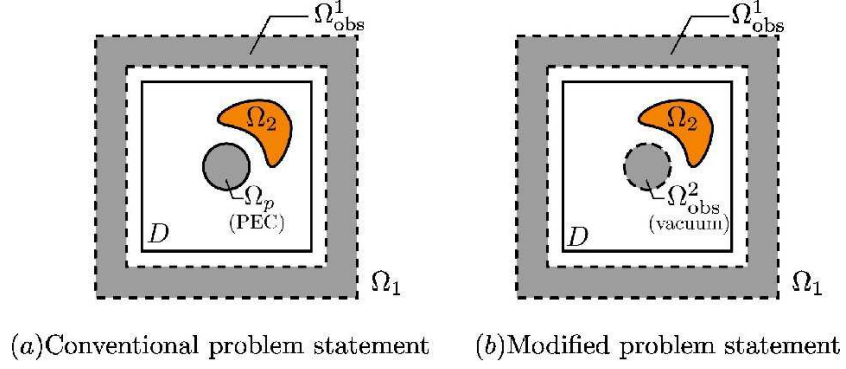


FIGURE 2. Two types of optimisation problems in design for cloaking devices.

**2.2. Expression of configuration with the level-set method.** We use the level-set method to express the configuration of a design object  $\Omega_2$ . In the level-set method, boundary of a design object  $\Gamma_d$  is expressed as zero-level contour of a level-set function  $\phi(\mathbf{x})$  defined in the design domain. Inner and outer domain of the design object is distinguished by the value of the level set function as follows:

$$(17) \quad \Omega_1 = \{ \mathbf{x} \mid 0 < \phi(\mathbf{x}) \leq 1 \},$$

$$(18) \quad \Gamma_d = \{ \mathbf{x} \mid \phi(\mathbf{x}) = 0 \},$$

$$(19) \quad \Omega_2 = \{ \mathbf{x} \mid -1 \leq \phi(\mathbf{x}) < 0 \}.$$

The value of  $\phi(\mathbf{x})$  is stored on a grid point of lattice expanding the design domain  $D$ . In order to generate a boundary mesh, we initially interpolate the value of the level-set function between neighbouring lattice points by a line. By connecting points at which  $\phi(\mathbf{x}) = 0$  in each lattice, boundary elements are generated (Figure 3). Generated boundary mesh by the above process may, however, includes boundary elements whose length are uneven. Hence, after the mesh generation, we improve these boundary elements so that the length of each boundary element becomes almost the same [18].

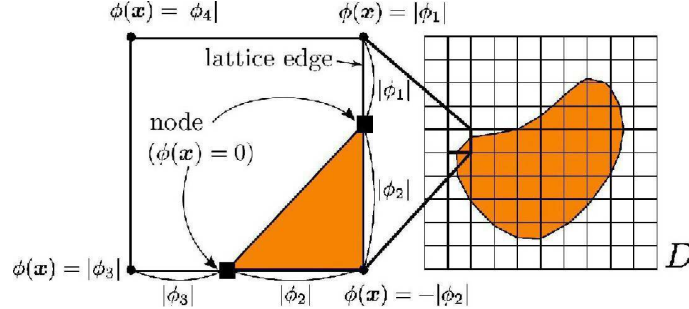


FIGURE 3. Generation of the boundary mesh.

**2.3. Update of configuration with the reaction-diffusion equation.** For the update of the level-set function at each optimisation step, we solve the following reaction-diffusion equation in the design domain  $D$  with appropriate initial and boundary conditions with respect to fictitious time  $t$  [14].

$$(20) \quad \frac{\partial \phi}{\partial t} = C \text{sgn}(\phi(\mathbf{x})) \mathcal{T}(\mathbf{x}) + \tau l^2 \nabla^2 \phi(\mathbf{x}).$$

In the right hand side (RHS) of equation (20), the first term denotes the direction and scale of the update of  $\phi(\mathbf{x})$ .  $C$  is a constant which arranges the scale.  $\mathcal{T}(\mathbf{x})$  denotes a topological derivative which is a sensitivity of the objective function with respect to new creation of an infinitesimal circular dielectric or vacuum domain. For the derivation of the topological derivative, the reader is referred to Section 3. The second term of the

RHS in equation (20) is so called Tikhonov's regularisation term and works as a perimeter constraint for a design object. By adjusting a parameter  $\tau$ , the complexity of obtained configuration after the update can be arranged [15].  $l$  is a characteristic length, in this study the side length of  $D$  is employed.

**2.4. Algorithm of the topology optimisation.** The algorithm of our topology optimisation is summarised as follows:

- Step 1: Initialise a level-set function in accordance with a initial configuration.
- Step 2: Generate a boundary mesh based on the level-set function (see Section 2.2).
- Step 3: Solve the boundary value problem (either (3)–(8) or (12)–(16)) with the BEM (see Section 4).
- Step 4: Compute the objective function and check if the convergence condition is satisfied or not. In this study we judge the objective function is converged at step  $k$  when the objective function of the last 50 steps ( $J_{k-49}, \dots, J_k$ ) satisfy the following relation:

$$(21) \quad J' \leq \varepsilon_1^{\text{conv}},$$

$$(22) \quad \max_{1 \leq i, j \leq 50} \left| \frac{J_{k-i+1}}{J_{k-j+1}} \right| \leq \varepsilon_2^{\text{conv}},$$

where  $J'$  denotes the gradient of the objective function which is evaluated with the least square for  $\log(J_{k-49}), \dots, \log(J_k)$ . Also,  $\varepsilon_1^{\text{conv}}, \varepsilon_2^{\text{conv}}$  are parameters. When the condition is satisfied, we terminate the optimisation process.

- Step 5: Compute the topological derivative derived in the Section 4.
- Step 6: Update the distribution of the level-set function by solving the reaction and diffusion equation (20) with the FEM (see Section 2.3) and back to the step 2.

### 3. TOPOLOGICAL DERIVATIVE

In our topology optimisation, we update a configuration of a design object iteratively based on a topological derivative (see the reaction-diffusion equation (20)); sensitivity of an objective function  $J$  when an infinitesimal circle  $\Omega_\varepsilon$  is allocated in a design domain  $D$  (Figure 4) [27]. In this section, we consider an objective function defined as summation of a function of  $u$  as follows:

$$(23) \quad J = \sum_{m=1}^M f(u(\mathbf{x}_m^{\text{obs}})),$$

where  $\mathbf{x}_m^{\text{obs}} \notin D$  ( $m = 1, \dots, M$ ) is an observation points. Other types of the objective function such as the one defined on the boundary can readily be obtained with a similar procedure as the following discussion.

Topological derivative is defined as a first coefficient in asymptotic expansion of the objective function by measure of the allocated infinitesimal circle  $s(\varepsilon)$  whose centre is  $\mathbf{x}$ :

$$(24) \quad \delta J = \mathcal{T}(\mathbf{x})s(\varepsilon) + o(s(\varepsilon)),$$

in which  $\delta J$  is a variation of the objective function which is evaluated as follows:

$$(25) \quad \begin{aligned} \delta J &= \frac{\partial J}{\partial u_r} \delta u_r + \frac{\partial J}{\partial u_i} \delta u_i \\ &= \Re \left[ \frac{\partial J}{\partial u} \delta u \right], \end{aligned}$$

where  $\delta u$  is a variation of the electric response when the infinitesimal circular domain is allocated on  $\mathbf{x}$ . Also, indices 'r' and 'i' represent the real part and imaginary part of  $\delta u$ , respectively. In the case that the allocated infinitesimal circle is made of dielectric element, it can easily be confirmed that  $\delta u$  satisfies the

following boundary value problem:

$$\begin{aligned}
(26) \quad & \nabla^2 \delta u(\mathbf{x}) + k_1^2 \delta u(\mathbf{x}) = 0 & \mathbf{x} \in \Omega_1, \\
(27) \quad & \nabla^2 \delta u(\mathbf{x}) + k_2^2 \delta u(\mathbf{x}) = 0 & \mathbf{x} \in \Omega_2, \\
(28) \quad & \nabla^2 \hat{u}(\mathbf{x}) + k_2^2 \hat{u}(\mathbf{x}) = 0 & \mathbf{x} \in \Omega_\varepsilon, \\
(29) \quad & \delta u_1 = \delta u_2 & \mathbf{x} \in \Gamma_d, \\
(30) \quad & \frac{1}{\mu_1} \left( \frac{\partial \delta u}{\partial n} \right)^1 = \frac{1}{\mu_2} \left( \frac{\partial \delta u}{\partial n} \right)^2 & \mathbf{x} \in \Gamma_d, \\
(31) \quad & \delta u = 0 & \mathbf{x} \in \Gamma_p, \\
(32) \quad & u_1 + \delta u_1 = \hat{u} & \mathbf{x} \in \Gamma_\varepsilon, \\
(33) \quad & \frac{1}{\mu_1} \frac{\partial (u_1 + \delta u_1)}{\partial n} = \frac{1}{\mu_2} \frac{\partial \hat{u}}{\partial n} & \mathbf{x} \in \Gamma_\varepsilon, \\
(34) \quad & \text{Radiation condition} & |\mathbf{x}| \rightarrow \infty,
\end{aligned}$$

where  $\hat{u}$  is the electro-magnetic response in  $\Omega_\varepsilon$ . We define the normal vector  $\mathbf{n}$  is positive when  $\mathbf{n}$  is directed from  $\Omega_1$ . In this study, we employ the adjoint variable method to evaluate the RHS of equation (25). Namely, we define the following adjoint problem:

$$\begin{aligned}
(35) \quad & \nabla^2 \tilde{u}(\mathbf{x}) + k_1^2 \tilde{u}(\mathbf{x}) + \sum_{m=1}^M \frac{\partial f(u(\mathbf{x}_m^{\text{obs}}))}{\partial u} \delta(\mathbf{x} - \mathbf{x}_m^{\text{obs}}) = 0 & \mathbf{x} \in \Omega_1, \\
(36) \quad & \nabla^2 \tilde{u}(\mathbf{x}) + k_2^2 \tilde{u}(\mathbf{x}) = 0 & \mathbf{x} \in \Omega_2, \\
(37) \quad & \tilde{u}^1 = \tilde{u}^2 & \mathbf{x} \in \Gamma_d, \\
(38) \quad & \frac{1}{\mu_1} \left( \frac{\partial \tilde{u}}{\partial n} \right)^1 = \frac{1}{\mu_2} \left( \frac{\partial \tilde{u}}{\partial n} \right)^2 & \mathbf{x} \in \Gamma_d, \\
(39) \quad & \tilde{u} = 0 & \mathbf{x} \in \Gamma_p, \\
(40) \quad & \text{Radiation condition} & |\mathbf{x}| \rightarrow \infty.
\end{aligned}$$

With the help of the reciprocal theorem for

- $\tilde{u}$  and  $\delta u$  in  $\Omega_1 \setminus \overline{\Omega_\varepsilon}$ ,
- $\tilde{u}$  and  $\delta u$  in  $\Omega_2$ ,
- $\tilde{u}$  and  $\hat{u}$  in  $\Omega_\varepsilon$ ,

the RHS of equation (25) is evaluated as follows:

$$(41) \quad \delta J = \Re \left[ \int_{\Omega_\varepsilon} \omega^2 (\varepsilon_2 - \varepsilon_1) \hat{u} \tilde{u} \, d\Omega \right].$$

The asymptotic behaviour of  $\hat{u}$  and  $\tilde{u}$  in  $\Omega_\varepsilon$  is evaluated as follows [27]:

$$(42) \quad \hat{u}(\mathbf{x}) = u(\mathbf{x}_0) + \frac{2\varepsilon_2}{\varepsilon_1 + \varepsilon_2} u_{,j}(\mathbf{x}_0) (\mathbf{x} - \mathbf{x}_0)_j + o(\varepsilon) \quad \mathbf{x} \in \Omega_\varepsilon,$$

$$(43) \quad \tilde{u}(\mathbf{x}) = \tilde{u}(\mathbf{x}_0) + \tilde{u}_{,j}(\mathbf{x}_0) (\mathbf{x} - \mathbf{x}_0)_j + o(\varepsilon) \quad \mathbf{x} \in \Omega_\varepsilon.$$

By substituting (42), (43) into (41), we obtain the following expression.

$$(44) \quad \delta J = \Re \left[ (\omega^2 (\varepsilon_2 - \varepsilon_1) \hat{u} \tilde{u}) \pi \varepsilon^2 + o(\varepsilon^2) \right].$$

From the definition (24), the topological derivative is derived as follows:

$$(45) \quad \mathcal{T}(\mathbf{x}) = \Re \left[ \omega^2 (\varepsilon_2 - \varepsilon_1) u(\mathbf{x}) \tilde{u}(\mathbf{x}) \right].$$

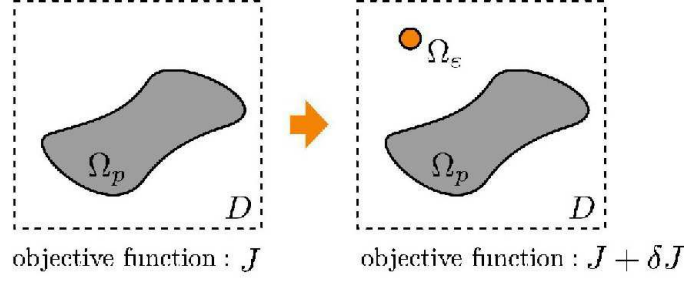


FIGURE 4. Allocation of an infinitesimal circle in the design domain.

#### 4. ELECTROMAGNETIC FIELD ANALYSIS IN THE 2D INFINITE DOMAIN

In this section, we show a method to solve two dimensional Maxwell's equations in the infinite domain which appears in the constraint in the optimisation problem (3)–(8) with the boundary element method (BEM). The BVP (12)–(16) can similarly be solved. The solution of the BVP (3)–(8) has the following integral representation:

$$(46) \quad u(\mathbf{x}) = u^{\text{inc}}(\mathbf{x}) - \int_{\Gamma_d} \frac{\partial G^1(\mathbf{x}, \mathbf{y})}{\partial n_y} u(\mathbf{y}) \, d\Gamma_y + \int_{\Gamma_p \cup \Gamma_d} G^1(\mathbf{x}, \mathbf{y}) \frac{\partial u(\mathbf{y})}{\partial n_y} \, d\Gamma_y \quad \mathbf{x} \in \Omega_1,$$

$$(47) \quad u(\mathbf{x}) = \int_{\Gamma_d} \frac{\partial G^2(\mathbf{x}, \mathbf{y})}{\partial n_y} u(\mathbf{y}) \, d\Gamma_y - \int_{\Gamma_d} G^2(\mathbf{x}, \mathbf{y}) \frac{\partial u(\mathbf{y})}{\partial n_y} \, d\Gamma_y \quad \mathbf{x} \in \Omega_2,$$

where  $G^i(\mathbf{x}, \mathbf{y})$  ( $i = 1, 2$ ) denotes the fundamental solution of the Helmholtz equation in 2D which is expressed by the Hankel function of the first kind of order 0 as follows:

$$(48) \quad G^i(\mathbf{x}, \mathbf{y}) = \frac{i}{4} H_0^{(1)}(k_i |\mathbf{x} - \mathbf{y}|).$$

By taking the limit as  $\mathbf{x} \rightarrow \Gamma_p$  and  $\Gamma_d$ , we can solve the obtained boundary integral equations. The obtained equations may, however, suffer from so called fictitious eigenfrequency problem. In order to avoid the problem, we employ the PMCHWT formulation [28] and obtain the following boundary integral equations:

$$(49) \quad \begin{bmatrix} -\mathcal{S}_1^{\Gamma_p} & \frac{1}{\mu_1} \mathcal{D}_1^{\Gamma_d} & -\mu_1 \mathcal{S}_1^{\Gamma_d} \\ -\mathcal{D}_1^{\Gamma_p} & \frac{\mathcal{N}_1^{\Gamma_d}}{\mu_1} + \frac{\mathcal{N}_2^{\Gamma_d}}{\mu_2} & -(\mathcal{D}_1^{\Gamma_d*} + \mathcal{D}_2^{\Gamma_d*}) \\ -\mu_1 \mathcal{S}_1^{\Gamma_p} & \mathcal{D}_1^{\Gamma_d} + \mathcal{D}_2^{\Gamma_d} & -(\mu_1 \mathcal{S}_1^{\Gamma_d} + \mu_2 \mathcal{S}_2^{\Gamma_d}) \end{bmatrix} \begin{bmatrix} w_p \\ u_d \\ w_d \end{bmatrix} = \begin{bmatrix} w_p^{\text{inc}} \\ w_d^{\text{inc}} \\ u_d^{\text{inc}} \end{bmatrix},$$

where indices 'p' and 'd' indicate the variable defined on  $\Gamma_p$  and  $\Gamma_d$ , respectively. Also,  $w_p$ ,  $w_p^{\text{inc}}$ ,  $w_d$  and  $w_d^{\text{inc}}$  are defined as follows:

$$(50) \quad w_p = \frac{1}{\mu_1} \left( \frac{\partial u}{\partial n} \right)^1,$$

$$(51) \quad w_p^{\text{inc}} = \frac{1}{\mu_1} u_p^{\text{inc}},$$

$$(52) \quad w_d = \frac{1}{\mu_1} \left( \frac{\partial u}{\partial n} \right)^1 = \frac{1}{\mu_2} \left( \frac{\partial u}{\partial n} \right)^2,$$

$$(53) \quad w_d^{\text{inc}} = \frac{1}{\mu_1} \frac{\partial u^{\text{inc}}}{\partial n}.$$

$\mathcal{D}_i^\Gamma$ ,  $\mathcal{S}_i^\Gamma$ ,  $\mathcal{D}_i^{\Gamma*}$  and  $\mathcal{N}_i^\Gamma$  respectively denote the following operators:

$$(54) \quad [\mathcal{D}_i^\Gamma \phi](\mathbf{x}) = \int_\Gamma \frac{\partial G^i(\mathbf{x}, \mathbf{y})}{\partial n_y} \phi(\mathbf{y}) \, d\Gamma_y,$$

$$(55) \quad [\mathcal{S}_i^\Gamma \psi](\mathbf{x}) = \int_\Gamma G^i(\mathbf{x}, \mathbf{y}) \psi(\mathbf{y}) \, d\Gamma_y,$$

$$(56) \quad [\mathcal{D}_i^{\Gamma*} \psi](\mathbf{x}) = \int_\Gamma \frac{\partial G^i(\mathbf{x}, \mathbf{y})}{\partial n_x} \psi(\mathbf{y}) \, d\Gamma_y,$$

$$(57) \quad [\mathcal{N}_i^\Gamma \phi](\mathbf{x}) = \int_\Gamma \frac{\partial^2 G^i(\mathbf{x}, \mathbf{y})}{\partial n_x \partial n_y} \phi(\mathbf{y}) \, d\Gamma_y,$$

where  $\phi$  and  $\psi$  are density functions. By discretising the boundary  $\Gamma_p \cup \Gamma_d$  and the electric field and magnetic field  $(u, w)$  in the boundary integral equation (49) by linear and constant element, respectively, the collocation gives the algebraic equations. After computing the electro-magnetic field on the boundary by solving the algebraic equations, we obtain the electric response in  $\Omega_1$  and  $\Omega_2$  by substituting the solutions on the boundary to equations (46) and (47), respectively.

## 5. EFFICIENT SENSITIVITY ANALYSIS WITH THE $\mathcal{H}$ -MATRIX METHOD

In the previous section, we showed the expression of the topological derivative with the adjoint variable method. For the computation of the topological derivative, we need to compute the electro-magnetic responses for two incident field; forward and adjoint. For the efficient computation of the topological derivative, fast direct solver is suitable since the coefficient matrix of forward and adjoint problem is the same, and we can solve these problems at the same time with a direct solver. The hierarchical matrix method; so called  $\mathcal{H}$ -matrix method is one of the promising acceleration methods for matrix operations [25, 26], and we can solve the algebraic equations with  $O(N \log N)$  computational cost by using accelerated LU decomposition with the  $\mathcal{H}$ -matrix method ( $\mathcal{HLU}$ ) in which  $N$  denotes the degree of freedom.

In the  $\mathcal{H}$ -matrix method, we firstly express a matrix in the form of the  $\mathcal{H}$ -matrix which is a matrix constructed through the following two steps:

- Hierarchical blocking of a matrix.
- Low rank approximation of submatrices which express influence from far field.

By applying efficient operations to each sub low rank matrices, the computational cost for matrix operations is reduced. In this section, we explain the construction of the  $\mathcal{H}$ -matrix following the above two steps. Also, we show an efficient sensitivity analysis method with the  $\mathcal{H}$ -matrix method.

**5.1. Blocking of a coefficient matrix.** As an example, we consider a vacuum domain  $\Omega_1$  in which some PEC objects  $\Omega_p$  are allocated. The boundary integral equation for this problem is derived as follows:

$$(58) \quad u^{\text{inc}}(\mathbf{x}) = - \int_{\Gamma_p} G^1(\mathbf{x}, \mathbf{y}) \frac{\partial u(\mathbf{y})}{\partial n_y} \, d\Gamma_y \quad \mathbf{x} \in \Gamma_p.$$

By discretising the boundary and  $\partial u / \partial n_y$  of (58) respectively with linear and constant element, we obtain a dense coefficient matrix  $A$  whose entry  $a_{ij}$  is expressed as follows:

$$(59) \quad a_{ij} = - \int_{\Gamma_j} G^1(\mathbf{x}_i, \mathbf{y}) \, d\Gamma_y,$$

where  $\Gamma_j$  denotes the  $j$ th discretised boundary element, and  $\mathbf{x}_i$  is the collocation point on  $\Gamma_i$ . One finds that each entry  $a_{ij}$  is associated with a collocation  $\mathbf{x}_i$  and a boundary element  $\Gamma_j$ . Hence, blocking of  $A$  can be done based on partition of  $\Gamma_p$ . Namely, we generate a boundary cluster and divide the coefficient matrix based on the clustering by the following strategy:

- Make a rectangle enclosing a boundary which we are going to be divided. We define a set of elements in the rectangle as a ‘cluster’. Also, we denote the number of division which is required to obtain the cluster as a ‘level’ to which the cluster belongs. In the following, we denote  $i$ th cluster in the level  $l$  as  $C_i^l$ .

- Divide the longer side of the rectangle into two parts. We define sets of elements in each obtained rectangle as new clusters (Figure 5). The coefficient matrix is also divided corresponding to the division of the boundary. Each block matrix corresponds to a combination of two clusters in the same level.
- When two clusters  $C_i^l$  and  $C_j^l$  at the same level  $l$  satisfy the following admissibility condition, we define the block matrix  $C_i^l \times C_j^l$  as an admissible block (the corresponding submatrix represents far-field influence) and stop dividing the block (Figure 5).

$$(60) \quad \min\{\text{diam } C_i^l, \text{diam } C_j^l\} \leq \eta \text{dist}\{C_i^l, C_j^l\},$$

where  $\eta$  denotes a real constant which sets the strictness of the condition (The larger  $\eta$  is set, the more blocks are recognised as admissible). ‘diam’ and ‘dist’ respectively denote diameter of a cluster and distance of two clusters (Figure 6) and defined as follows:

$$(61) \quad \text{diam } C_i^l = \max_{\mathbf{x}, \mathbf{y} \in C_i^l} |\mathbf{x} - \mathbf{y}|,$$

$$(62) \quad \text{dist}\{C_i^l, C_j^l\} = \min_{\mathbf{x} \in C_i^l, \mathbf{y} \in C_j^l} |\mathbf{x} - \mathbf{y}|.$$

- We repeat the above process until the number of nodes in each cluster is less than a preset parameter  $n_{\min}$ . We define such clusters as ‘leaf cluster’. When at least one of two clusters  $C_s^l, C_t^l$  at the same level  $l$  is a leaf cluster and  $C_s^l, C_t^l$  does not satisfy the admissibility condition (60), we define the block  $C_s^l \times C_t^l$  as an inadmissible block (the corresponding submatrix represents near-field influence).

After we obtain the structure of the  $\mathcal{H}$ -matrix, we compute the submatrices corresponding to inadmissible and admissible blocks. While the inadmissible matrices are calculated according to its definition (59), the admissible counterparts are evaluated in a low rank approximated form which is presented in the following subsection.

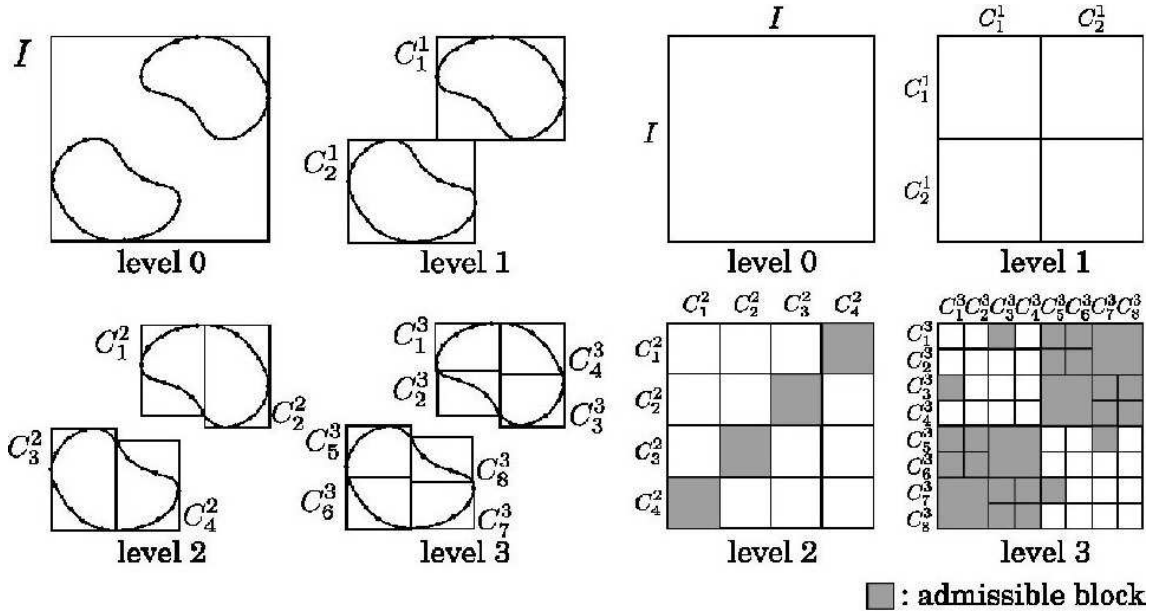


FIGURE 5. An example of boundary clustering and corresponding division of a coefficient matrix.

**5.2. Efficient computation of block matrices with the ACA and parallelisation.** Low rank approximation is a method to express a matrix  $A \in \mathbb{C}^{m \times n}$  with two vectors  $\mathbf{a}_l \in \mathbb{C}^{m \times 1}$  and  $\mathbf{b}_l \in \mathbb{C}^{n \times 1}$

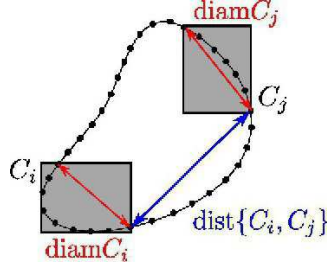


FIGURE 6. Definition of diam and dist.

( $l = 1, \dots, k$ ) as follows:

$$(63) \quad A \simeq S_k = \sum_{i=1}^k \mathbf{a}_i \mathbf{b}_i^H,$$

where  $S_k$  is an approximation matrix of  $A$ , and  $k$  is the rank of  $S_k$ . Although the original matrix  $A$  requires  $O(mn)$  memory to store the matrix, approximated matrix  $S_k$  requires  $O(k(m+n))$  memory. Hence, when the rank  $k$  satisfies  $k < mn/(m+n)$  we can reduce the memory consumption. Also, we can define efficient matrix operations such as matrix-vector product, LU decomposition, etc for matrices expressed in the form of (63).

The adaptive cross approximation (ACA) is one of the techniques to realise the low-rank approximation (63) of matrices. The algorithm of the ACA is shown in Algorithm 1. For more details such as the selection of the initial row and efficient evaluation of the Frobenius norm etc, the reader may consult [29].

As a result of approximation with the ACA, the approximation matrix satisfies the following error estimation:

$$(64) \quad \|A - S_k\|_F \leq \varepsilon \|A\|_F,$$

where  $\|\cdot\|_F$  denotes the Frobenius norm, and  $\varepsilon$  is a tolerance for the ACA. In the algorithm of the ACA, we need not to compute all of the entries of  $A$ , which can reduce the assemble cost of the coefficient matrix.

---

**Algorithm 1** Adaptive cross approximation (ACA)

---

```

Let  $i_1 = \text{Initial Row}$ 
for  $k = 1$  to  $m$  do
   $\mathbf{b}_k = A(i_k, :) - \sum_{l=1}^{k-1} (\mathbf{a}_l)_{i_k} \mathbf{b}_l$ 
   $j_k = \text{argmax}(|(\mathbf{b}_k)_j|)$ 
   $\mathbf{a}_k = A(:, j_k) - \sum_{l=1}^{k-1} (\mathbf{b}_l)_{j_k} \mathbf{a}_l$ 
   $\mathbf{a}_k = (\mathbf{b}_k)^{-1} \mathbf{a}_k$ 
  if ( $\|\mathbf{a}_k\|_F \|\mathbf{b}_k\|_F \leq \varepsilon \|A_k\|_F$ ) then
    exit
  end if
   $i_{k+1} = \text{argmax}(|(\mathbf{a}_k)_i|)$ 
end for

```

---

For further acceleration of the  $\mathcal{H}$ -matrix generation process, we consider to parallelise the procedure. Since the admissible and inadmissible matrices can separately be computed, we can parallelise the process to generate the  $\mathcal{H}$ -matrix. To achieve high parallel performance, however, we need to carefully distribute the tasks to each thread because the size of each block matrix may differ from each other. In this study, the block matrices are stuck in descending order in size and the block matrices are distributed to threads with dynamic scheduling. In the dynamic scheduling, all the threads share the list of tasks. When we use  $n$  threads for the parallelisation,  $n$  tasks from top of the list are firstly distributed to each thread. When a thread finish its assigned task, the thread gets a new one from top of the list of unprocessed tasks. By this scheduling, we can keep almost all of the threads running and improve the parallel performance.

**5.3. Improvement of the  $\mathcal{H}$ -matrix structure by the agglomeration.** In the  $\mathcal{H}$ -matrix method, we sometimes are required to refine a  $\mathcal{H}$ -matrix structure since the computational cost for the  $\mathcal{H}$ LU will increase in accordance with fineness of the  $\mathcal{H}$ -matrix. The agglomeration is a technique to refine a  $\mathcal{H}$ -matrix by approximating four matrix as one low rank matrix. As an example, we consider the following matrix  $A \in \mathbb{C}^{m \times n}$  constructed by four low rank matrices:

$$(65) \quad A = \begin{bmatrix} U_1 V_1^H & U_3 V_3^H \\ U_2 V_2^H & U_4 V_4^H \end{bmatrix},$$

where  $U_i$  ( $i = 1, \dots, 4$ ) (resp.  $V_i$ ) denote a matrix whose size is  $m \times k_i$  (resp.  $n \times k_i$ ) with the rank  $k_i$ . In the agglomeration, we firstly express  $A$  as a product of two matrices  $U \in \mathbb{C}^{m \times 2n}$  and  $V \in \mathbb{C}^{n \times 2n}$  as follows:

$$(66) \quad A = UV^H = \begin{bmatrix} U_1 & U_3 \\ U_2 & U_4 \end{bmatrix} \begin{bmatrix} V_1 & V_2 \\ V_3 & V_4 \end{bmatrix}^H.$$

In order to approximate the matrix  $A$  as a low rank matrix, we apply the QR decomposition to  $U$ ,  $V$  and obtain the following expression of  $A$ :

$$(67) \quad A = Q_U R_U R_V^H Q_V^H.$$

With the help of the singular value decomposition of  $R_U R_V^H$ ,  $A$  is expressed in the form of  $U' \Sigma V'$  in which  $U' \in \mathbb{C}^{m \times m}$ ,  $V' \in \mathbb{C}^{n \times n}$  denote orthogonal matrices, and  $\Sigma \in \mathbb{C}^{m \times n}$  denote a diagonal matrix with singular values on the diagonal. By rounding singular values less than a preset value, we approximate  $A$  as a low rank matrix.

**5.4. Acceleration of the sensitivity analysis with the  $\mathcal{H}$ -matrix method.** With the help of the  $\mathcal{H}$ -matrix method, we can reduce the computational cost to solve the algebraic equations to  $O(N \log N)$  for the number of boundary elements  $N$  by the LU decomposition. The accelerated LU decomposition with the  $\mathcal{H}$ -matrix method is henceforth denoted as  $\mathcal{H}$ LU. In this study, we further accelerate the sensitivity analysis by solving the forward problem (3)–(8) and adjoint problem (35)–(40) at one time with the  $\mathcal{H}$ LU.

Furthermore, we consider to accelerate the computation of the electro-magnetic response in the domain  $\Omega_1$ ,  $\Omega_2$  and adjoint incident field by the fast matrix-vector multiplication with the  $\mathcal{H}$ -matrix method. The TM polarised electro-magnetic response in each domain is summarised as follows:

$$(68) \quad \begin{bmatrix} u(\mathbf{x}) \\ \frac{\partial u(\mathbf{x})}{\partial x_1} \\ \frac{\partial u(\mathbf{x})}{\partial x_2} \end{bmatrix} = \begin{bmatrix} \mu_1 S_1^{\Gamma_p} & -D_1^{\Gamma_d} & \mu_1 S_1^{\Gamma_d} \\ \mu_1 D_{1,1}^{\Gamma_p*} & -N_{1,1}^{\Gamma_d} & \mu_1 D_{1,1}^{\Gamma_d*} \\ \mu_1 D_{1,2}^{\Gamma_p*} & -N_{1,2}^{\Gamma_d} & \mu_1 D_{1,2}^{\Gamma_d*} \end{bmatrix} \begin{bmatrix} w_p \\ u_d \\ w_d \end{bmatrix} \quad \mathbf{x} \in \Omega_1,$$

$$(69) \quad \begin{bmatrix} u(\mathbf{x}) \\ \frac{\partial u(\mathbf{x})}{\partial x_1} \\ \frac{\partial u(\mathbf{x})}{\partial x_2} \end{bmatrix} = \begin{bmatrix} D_2^{\Gamma_d} & -\mu_2 S_2^{\Gamma_d} \\ N_{2,1}^{\Gamma_d} & -\mu_2 D_{2,1}^{\Gamma_d*} \\ N_{2,2}^{\Gamma_d} & -\mu_2 D_{2,2}^{\Gamma_d*} \end{bmatrix} \begin{bmatrix} u_d \\ w_d \end{bmatrix} \quad \mathbf{x} \in \Omega_2,$$

where,  $D_{i,j}^{\Gamma*}$  and  $N_{i,j}^{\Gamma}$  respectively denote the following operators:

$$(70) \quad [D_{i,j}^{\Gamma*} \psi](\mathbf{x}) = \int_{\Gamma} \frac{\partial G^i(\mathbf{x}, \mathbf{y})}{\partial x_j} \psi(\mathbf{y}) \, d\Gamma_y,$$

$$(71) \quad [N_{i,j}^{\Gamma} \phi](\mathbf{x}) = \int_{\Gamma} \frac{\partial^2 G^i(\mathbf{x}, \mathbf{y})}{\partial x_j \partial n_y} \phi(\mathbf{y}) \, d\Gamma_y.$$

The incident field of adjoint problem is also summarised as matrix vector multiplication as follows:

$$(72) \quad \begin{bmatrix} \tilde{u}^{\text{inc}}(\mathbf{x}_1) \\ \vdots \\ \tilde{u}^{\text{inc}}(\mathbf{x}_n) \end{bmatrix} = \begin{bmatrix} G^1(\mathbf{x}_1, \mathbf{x}_1^{\text{obs}}) & \cdots & G^1(\mathbf{x}_1, \mathbf{x}_m^{\text{obs}}) \\ \vdots & \ddots & \vdots \\ G^1(\mathbf{x}_n, \mathbf{x}_1^{\text{obs}}) & \cdots & G^1(\mathbf{x}_n, \mathbf{x}_m^{\text{obs}}) \end{bmatrix} \begin{bmatrix} \frac{\partial f}{\partial u}(\mathbf{x}_1^{\text{obs}}) \\ \vdots \\ \frac{\partial f}{\partial u}(\mathbf{x}_m^{\text{obs}}) \end{bmatrix} \quad \mathbf{x} \in \Omega_1,$$

in which  $\mathbf{x}_i$  ( $i = 1, \dots, n$ ) denotes the points at which we compute the adjoint incident field. We reduce the computational cost for assembling the coefficient matrices and matrix vector multiplication with the  $\mathcal{H}$ -matrix method and the ACA.

## 6. NUMERICAL EXAMPLES

In this section, we show the effectiveness of the proposed method by some numerical examples.

As the first numerical example, we investigate the computational cost for the  $\mathcal{H}$ LU, computation of the electro-magnetic response in the domain  $\Omega_1 \cap D$ ,  $\Omega_2$  and computation of the adjoint incident field. We consider a single step of an optimisation problem to minimise the amount of scattered field at some observation points allocated in a lattice form around a fixed design domain for an incident field which propagates in the  $x$ -direction (Figure 7). The number of observation points is 2290, and the distance between neighbouring observation points is fixed to 2.5. We compare the computational cost to solve the forward and adjoint problems on the boundary of a dielectric elements shown in Figure 7 with the  $\mathcal{H}$ LU and compare it with that for the GMRES accelerated by the FMM (FMGMRES) and GMRES without acceleration. Note that since FMGMRES and GMRES are iterative solver, the forward and adjoint problems are solved individually. On the other hand, since the  $\mathcal{H}$ LU is a direct solver, the LU decomposition of the coefficient matrix can be used for both forward and adjoint analysis.

The tolerance for  $\mathcal{H}$ -matrix operations and the ACA are set to  $\varepsilon = 10^{-5}$  in this study, which is determined in a way such that relative error by the  $\mathcal{H}$ -matrix method for the solution on the boundary of a dielectric circle is negligible compared to the discretisation error. Also, through some numerical experiments, we employ  $\eta = 128$  and  $n_{\text{min}} = 128$  which reduce the computational cost for numerical analyses most efficiently. Tolerance of the GMRES is set to  $10^{-5}$ . In every examples, we use the agglomeration technique when we generate a  $\mathcal{H}$ -matrix. Figure 8 shows the computational time for the number of boundary elements  $N = 600, 1200, 2400, 4800, 9600$  when  $\varepsilon_2$  is either 2 or 5 or 8. The number of iteration with the GMRES in the case of  $N = 600$  is attached to each figure as  $n_{\text{itr}}$ .  $\mathcal{H}$ LU achieves almost  $O(N \log N)$  computational cost in every cases. Through the comparison between the result for different  $\varepsilon_2$ , one observes that computational cost for FMGMRES and GMRES increase in association with increase of  $\varepsilon_2$  due to deterioration of convergence property, while that for  $\mathcal{H}$ LU is almost the same independently on  $\varepsilon_2$ . As for the complexity of dielectric element shape,  $\mathcal{H}$ LU shows stable computational time when  $N$  is around 1000. On the other hand, for larger  $N$  the computational time get to be sensitive to the complexity of shape for all of solvers. The computational time for the inner computation (68) and (69) in forward and adjoint problem for the same parameters with the previous result is shown in Figure 9. Also, Table 1 shows the computational time for the computation of the adjoint incident field on the boundary and inner points for  $N = 9600$ . Both results indicate that the FMM is the fastest for a simple matrix-vector multiplication. The  $\mathcal{H}$ -matrix method also achieve the fast computation compared to the case without acceleration. One observes that the result for the FMM does not shows monotonous increase in accordance with  $N$ . This is because parameters for the FMM is chosen in a way that the computational time for whole sensitivity analysis is the fastest.

Next, we apply the proposed method to the conventional topology optimisation problem (1)–(8) of cloaking devices. We consider to determine configuration of cloaking devices which make a circular PEC invisible for a TM polarised plane incident field. The radius of PEC is fixed to 10.0 in this example. We consider a design domain  $D$  whose size is  $[0, 100] \otimes [0, 100]$  (Figure 10). We allocate 2290 observation points  $\mathbf{x}_m^{\text{obs}}$  ( $m = 1, \dots, 2290$ ) on each lattice points in an observation domain  $\Omega_{\text{obs}}$  around  $D$  and define the objective function by equation (1) as sum of the scattered field on the observation points. We firstly determine the initial configuration  $\Omega_2^{\text{init}}$  as follows:

$$(73) \quad \Omega_2^{\text{init}} = \{ \mathbf{x} \mid \mathcal{T}^0(\mathbf{x}) \leq 0, \|\mathbf{x} - (50, 50)^T\|_2 \leq 50 \},$$

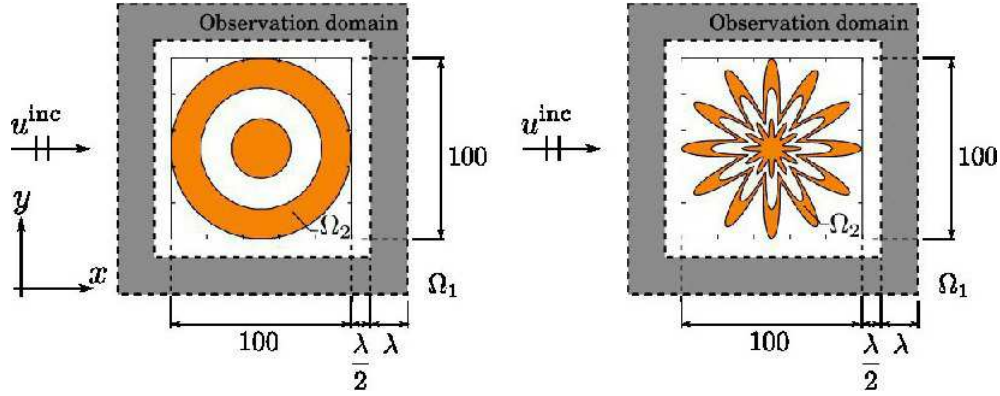


FIGURE 7. Problem statement for the test of performance of the  $\mathcal{H}$ -matrix method.

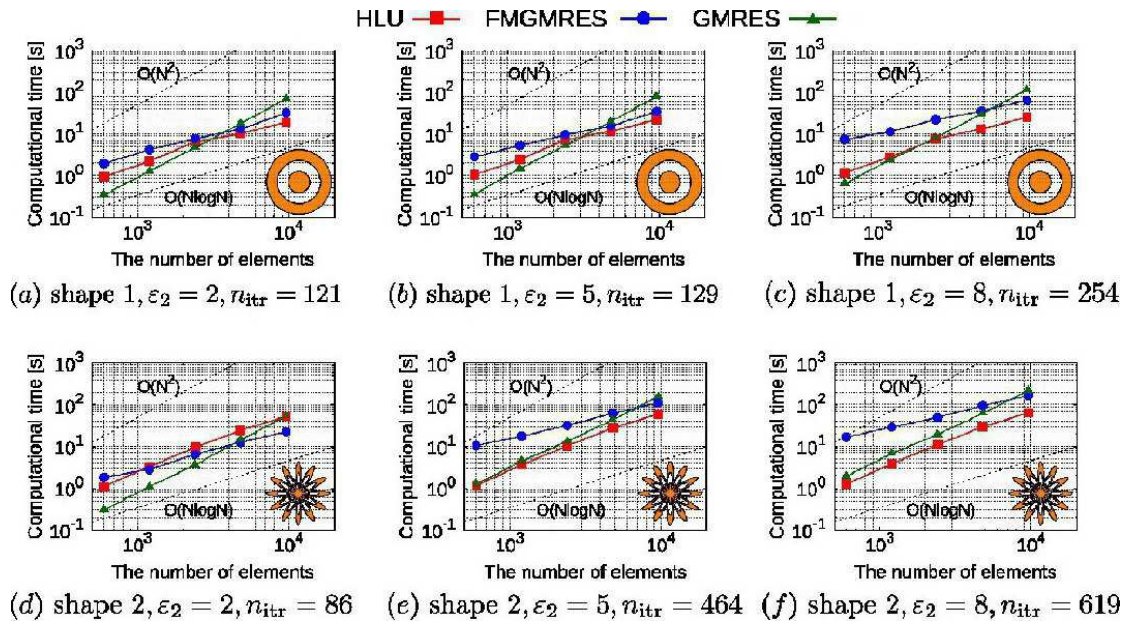


FIGURE 8. Computational time to compute the forward and adjoint response on the boundary of dielectric elements attached to each figure. Permittivity of dielectric elements  $\varepsilon_2$  and the number of iteration  $n_{itr}$  for GMRES when  $N$  equals to 600 are inserted.

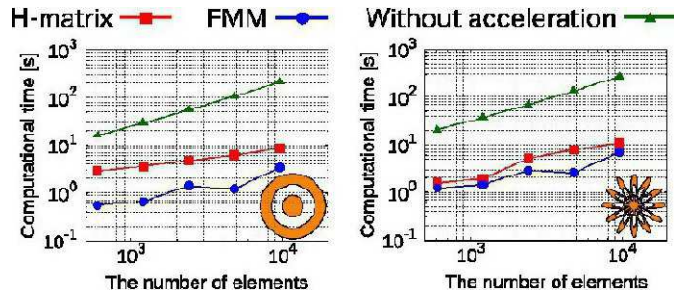


FIGURE 9. Computational time for the inner computation for  $\varepsilon_2 = 2$ .

TABLE 1. Computational time for the adjoint incident field for  $\varepsilon_2 = 2$ .

	Shape 1	Shape 2
$\mathcal{H}$ -matrix method	0.45 [s]	0.40 [s]
FMM	0.13 [s]	0.18 [s]
Without acceleration	9.80 [s]	9.44 [s]

where  $\mathcal{T}^0(\mathbf{x})$  denotes the topological derivative when only circular PEC is allocated in the design domain (10).

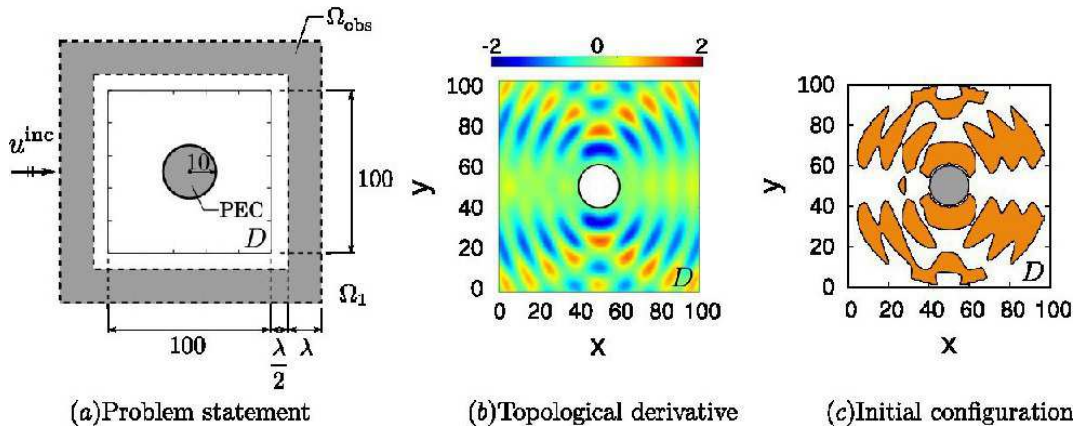


FIGURE 10. (a) Conventional problem statement, (b) The topological derivative when only circular PEC is allocated in the design domain, (c) The initial configuration determined by the sign of the topological derivative (b) at each point.

In the following results, the value of the objective function is normalised by the one when only circular PEC is allocated, which is denoted as  $J_1$ . The history of the objective function for  $\tau = 5.0 \times 10^{-3}$  and  $\varepsilon_2 = 2.0$  is shown in Figure 11. The objective function is successfully reduced as the optimisation step goes. For the optimal configuration, the objective function is reduced to approximately 0.11% of the original objective function when only circular PEC is allocated. The initial shape, optimal configurations and the electric field for  $\tau = 5.0 \times 10^{-3}, 1.0 \times 10^{-2}, 2.0 \times 10^{-2}$ ,  $\varepsilon_2 = 2$  (resp.  $\varepsilon_2 = 5$ ) are shown in Figure 12 (resp. Figure 13). For the initial configuration, the electric field is highly affected by scattered field. On the other hand, the optimal configurations for  $\tau = 5.0 \times 10^{-3}$  successfully reduce the scattering around the PEC and dielectric elements. One observes that complexity of the optimal configuration is reduced corresponding to the increase of  $\tau$  while the objective function for the optimal configuration becomes larger. Figure 14 shows comparison of the computational time for the sensitivity analysis with the  $\mathcal{H}$ LU and that with the FMGMRES at each optimisation step. One observes that computational time for FMGMRES is sensitive to the change of the permittivity  $\varepsilon_2$ , while the  $\mathcal{H}$ LU takes almost the same cost for the sensitivity analysis independently on  $\varepsilon_2$ . Total computational time to obtain the optimal configuration with the  $\mathcal{H}$ LU for  $\varepsilon_2 = 5$  is reduced to 58.7% of that with the FMGMRES.

In order to check the dependency of the cloaking effect on shape and material of a target object, we show the distribution of the electric field when various shape of PEC or dielectric material is allocated in the obtained cloaking device for  $\varepsilon_2 = 2$ ,  $\tau = 5.0 \times 10^{-3}$  (Figure 15). One observes that the value of the objective function differs by the shape and material of the target objects, and obtained design does not work as a cloaking device for target objects except for circular PEC.

In the next example, we redefine the objective function by (10) as sum of the electric field in a fixed circle  $\Omega_{obs}^1$  whose radius is 12.0 at the center of the design domain and the scattered field in  $\Omega_{obs}^2$  which is the same

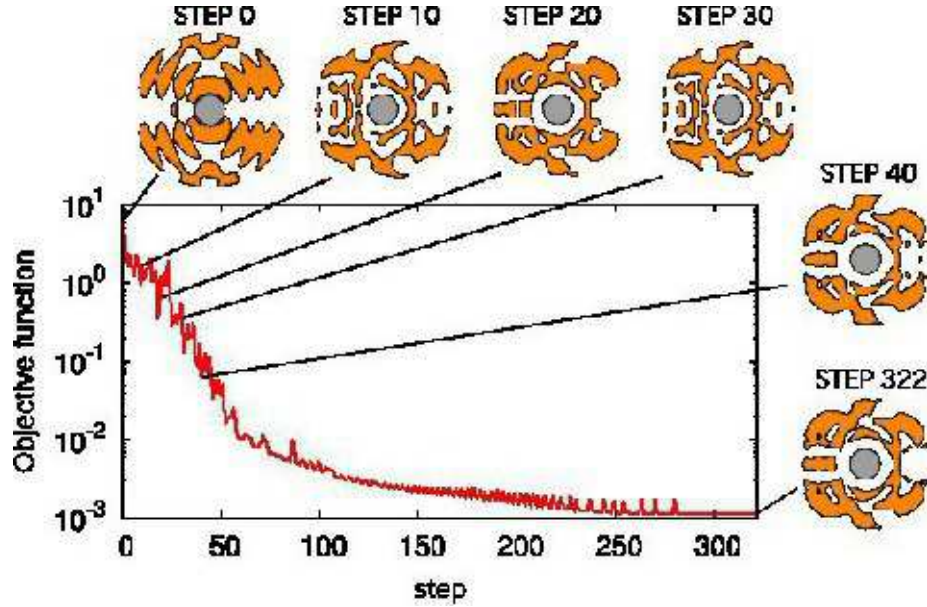


FIGURE 11. The history of the objective function and configuration of dielectric elements for  $\varepsilon_2 = 2$ ,  $\tau = 5.0 \times 10^{-3}$ .

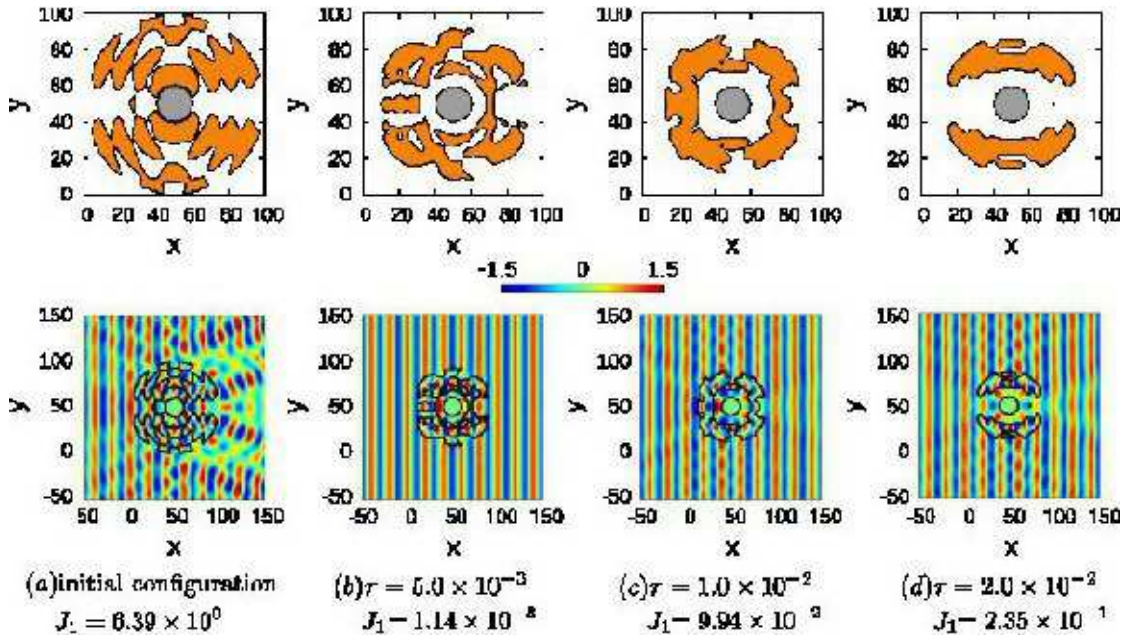


FIGURE 12. The initial configuration (a) and the optimal configuration (b)–(c) with the electric responses for the conventional optimisation problem in the case of  $\varepsilon_2 = 2$ .

domain with  $\Omega_{\text{obs}}$  in the previous example (Figure 16). We put 437 observation points on lattice points in  $\Omega_{\text{obs}}^1$  in a way that the distance between neighbouring points is 1 in addition to the 2290 observation points in  $\Omega_{\text{obs}}^2$ . The initial configuration is obtained by redefining  $\mathcal{T}^0(x)$  in the equation (73) as the topological derivative when nothing is put in the design domain (Figure 16).

In the following results, we denote the objective function which is normalised by the one when nothing is put in the design domain as  $J_2$ . Obtained configuration of dielectric elements and distribution of the

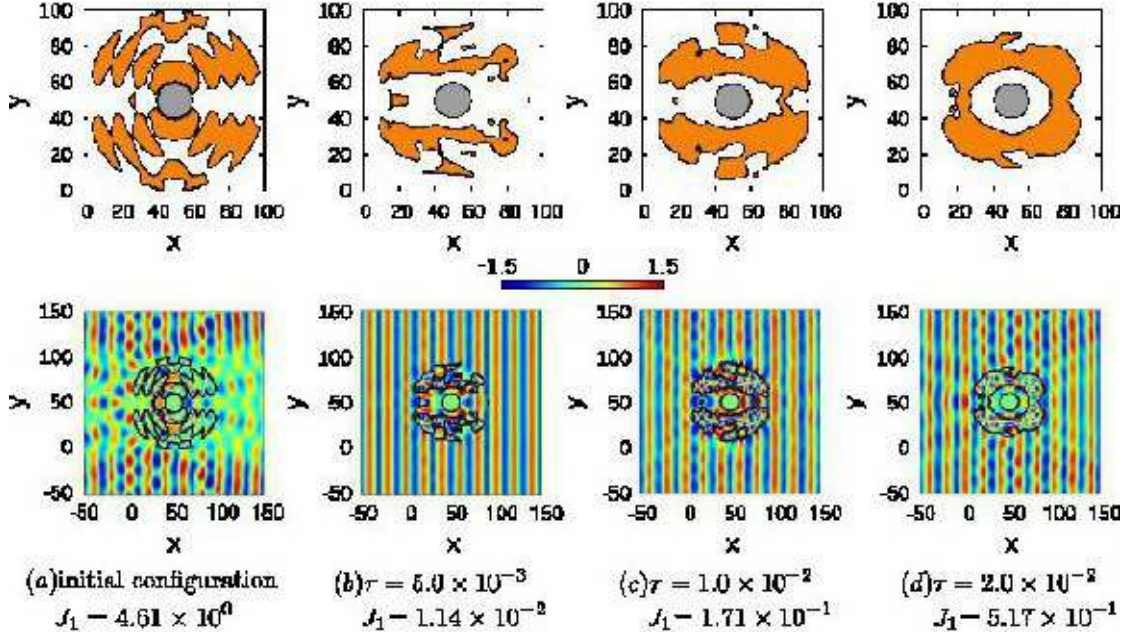


FIGURE 13. The initial configuration (a) and the optimal configuration (b)–(c) with the electric responses for the conventional optimisation problem in the case of  $\varepsilon_2 = 5$ .

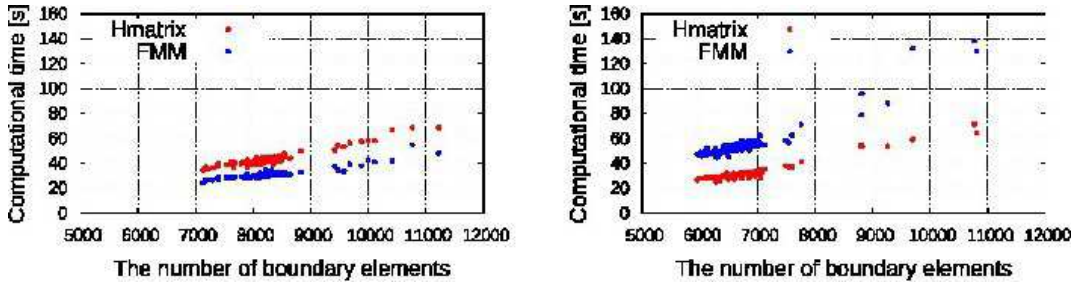


FIGURE 14. Computational time for the sensitivity analysis at each step of the conventional optimisation problem for  $\tau = 5.0 \times 10^{-3}$ ,  $\varepsilon_2 = 2$  (left) and 5 (right).

electric field for  $\varepsilon_2 = 2$  and 5 are shown in Figure 17 and Figure 18, respectively. In both cases, the optimal configuration for  $\tau = 5.0 \times 10^{-3}$  successfully reduces the electric field in  $\Omega_{\text{obs}}^1$  in addition to the scattered field in  $\Omega_{\text{obs}}^2$ . As with the previous example, one finds that higher value of  $\tau$  leads more simple configuration and larger objective function. Computational time for the sensitivity analysis at each optimisation step (Figure 19) shows that the  $\mathcal{H}\text{LU}$  works stably independently on  $\varepsilon_2$  compared to the FMGMRES. Figure 20 shows the electric response of the optimal configuration for  $\varepsilon_2 = 5$  and  $\tau = 5.0 \times 10^{-3}$  when various shape of PEC or dielectric element is allocated in  $\Omega_{\text{obs}}^2$ . For the comparison with the previous result Figure 15, the value of the objective function  $J_1$  defined by the conventional manner is attached. The result indicates that the obtained cloaking design works successfully independently on the shape and material of the hidden object.

## 7. CONCLUSION

We developed the topology optimisation method of cloaking devices which work for arbitrary-shaped target object with efficient and accurate sensitivity analysis using the BEM and the  $\mathcal{H}$ -matrix method. By the proposed method, we obtained structure of cloaking devices with low computational cost and confirmed that it works successfully independently on the shape of perfect electric conductor allocated in the cloaking

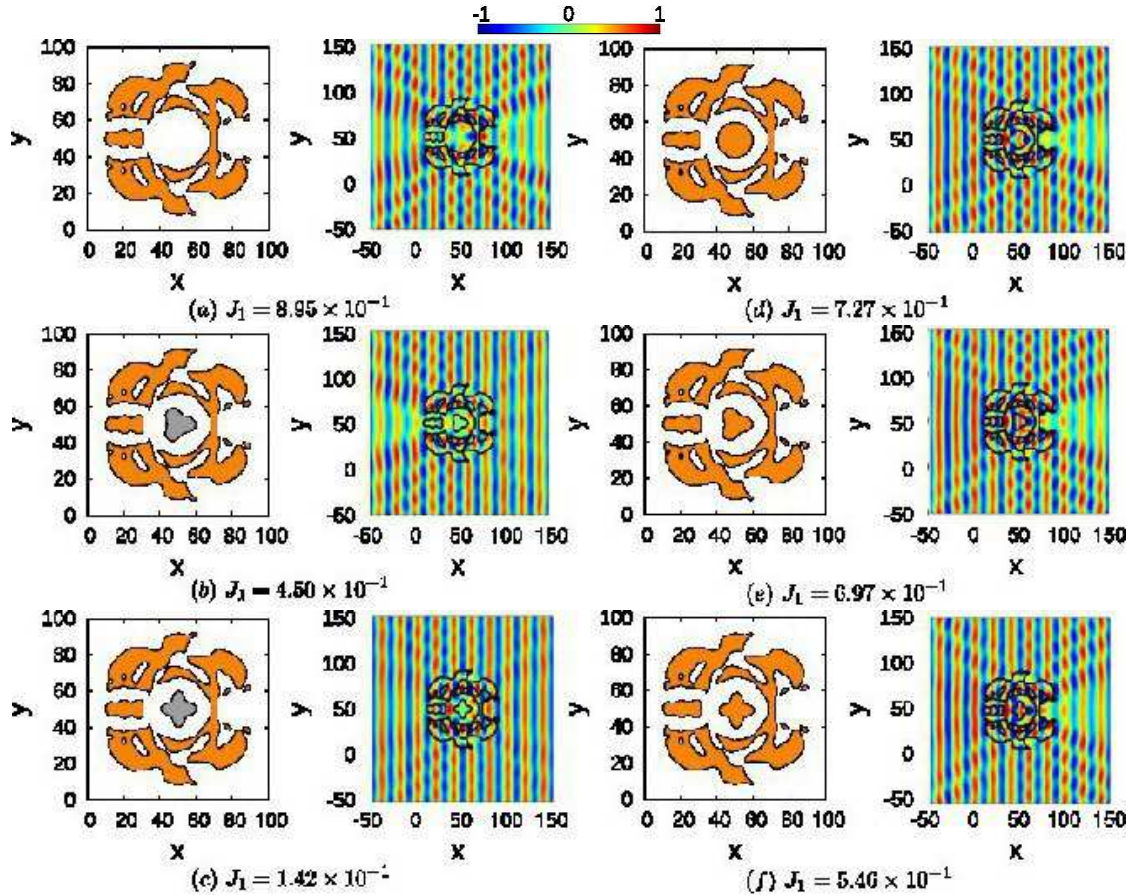


FIGURE 15. The electric field when nothing is put (a), some shapes of PEC are put (b), (c) and some shapes of dielectric element are put (d)–(f) in the cloaking device obtained by the conventional optimisation problem with  $\varepsilon_2 = 2$ ,  $\tau = 5.0 \times 10^{-3}$ .

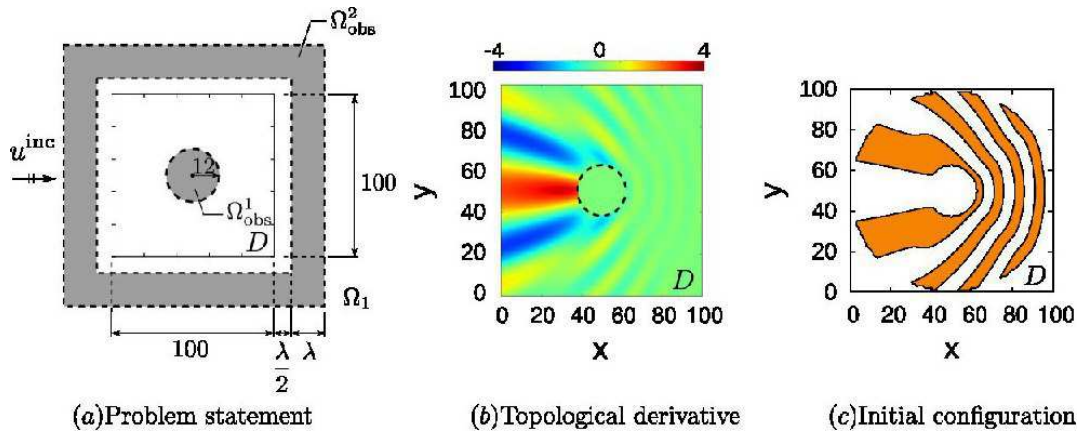


FIGURE 16. (a) Modified problem statement, (b) The topological derivative when nothing is allocated in the design domain, (c) The initial configuration determined by the sign of the topological derivative (b) at each point.

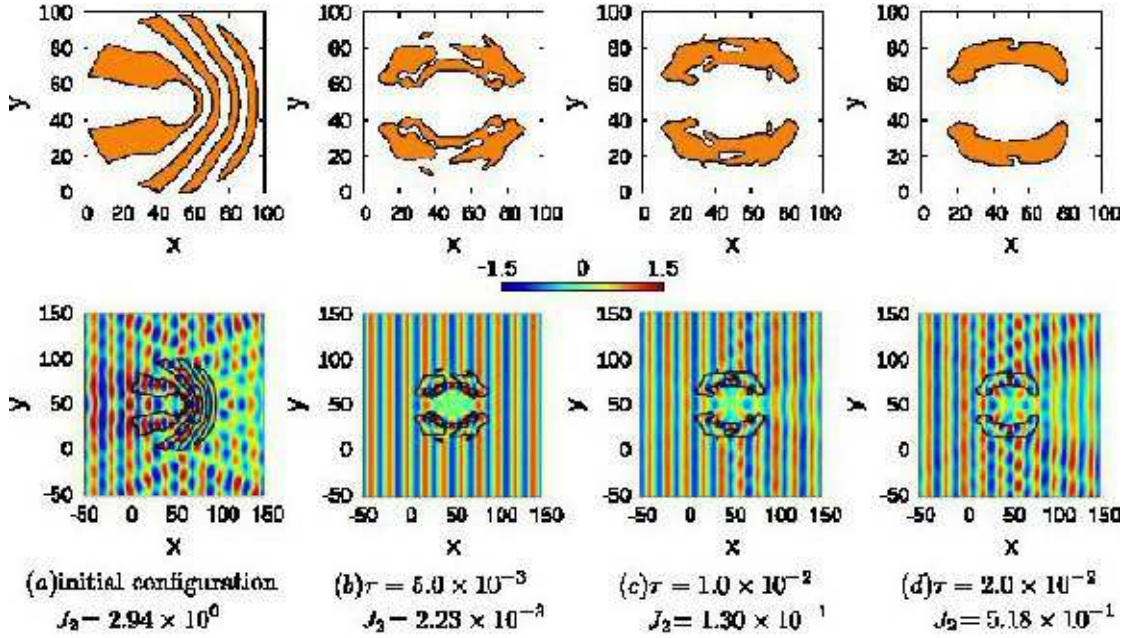


FIGURE 17. The initial configuration (a) and the optimal configuration (b)–(c) with the electric responses for the modified optimisation problem in the case of  $\varepsilon_2 = 2$ .

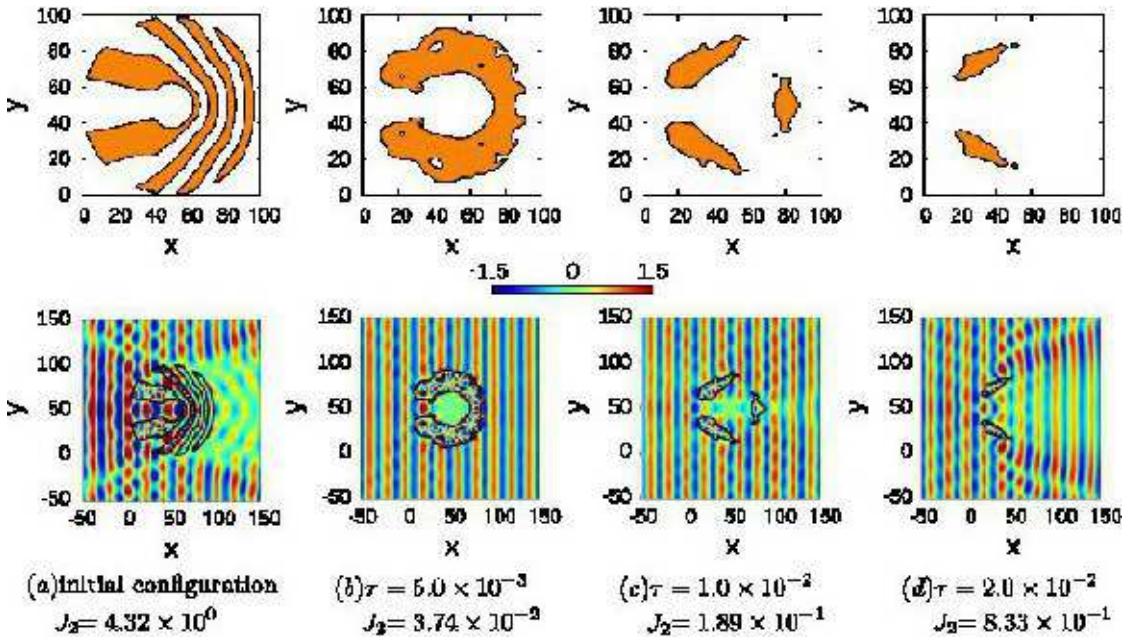


FIGURE 18. The initial configuration (a) and the optimal configuration (b)–(c) with the electric responses for the modified optimisation problem in the case of  $\varepsilon_2 = 5$ .

device. As a future task, we consider to extend the proposed method to the 3D problem. In 3D cases, the numerical cost for the electro-magnetic field analysis will be a key factor for the topology optimisation. Hence, we firstly try to develop a fast BEM with the  $\mathcal{H}$ -matrix method for the Maxwell's equations. Also, in 3D problems, the memory consumption to memorise the matrix for the inner computation will be huge. Hence, we need to develop an efficient algorithm to reduce the memory consumption.

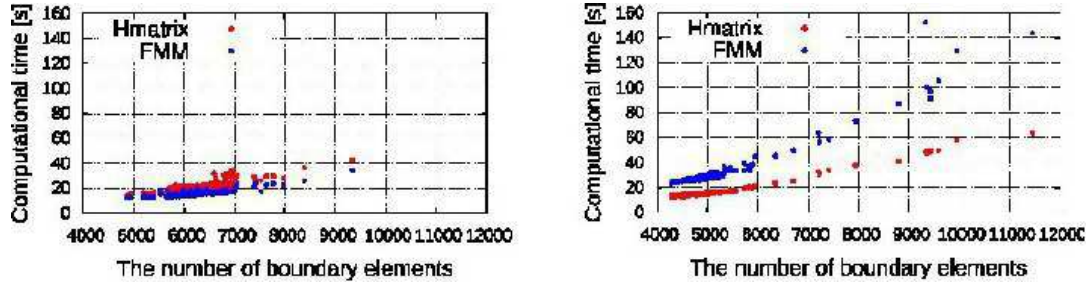


FIGURE 19. Computational time for the sensitivity analysis at each step of the modified optimisation problem for  $\tau = 5.0 \times 10^{-3}$ ,  $\varepsilon_2 = 2$  (left) and 5 (right).

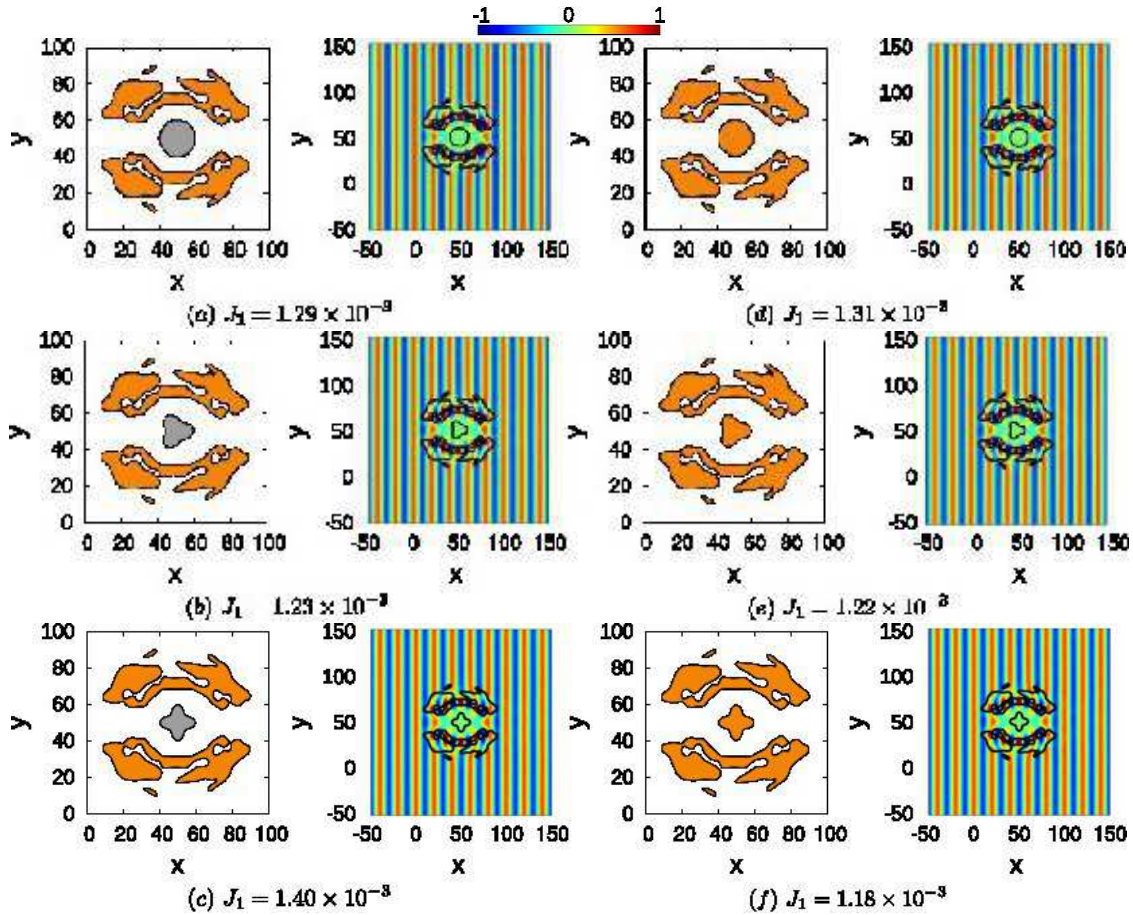


FIGURE 20. The electric field when nothing is put (a), some shapes of PEC are put (b), (c) and some shapes of dielectric element are put (d)–(f) in the cloaking device obtained by the modified optimisation problem with  $\varepsilon_2 = 2$ ,  $\tau = 5.0 \times 10^{-3}$ .

#### REFERENCES

- [1] Pendry JB, Holden AJ, Robbins DJ, Stewart WJ. Magnetism from Conductors and Enhanced Nonlinear Phenomena. *IEEE Transactions on microwave theory and techniques* 1999; **47**(11):2075–2084.
- [2] Hrbar S, Bartolic J, Sipus Z. Waveguide Miniaturization Using Uniaxial Negative Permeability Metamaterial. *IEEE Transactions on antennas and propagation* 2005; **53**(1):110–119.
- [3] Fang N, Zhang X. Imaging properties of a metamaterial superlens. *Applied physics letters* 2003; **82**(2):161–163.
- [4] Pendry JB, Schurig D, Smith DR. Controlling Electromagnetic Fields. *Science* 2006; **312**(5781):1780–1782.

- [5] Schurig D, Mock JJ, Justice BJ, Cummer SA, Pendry JB, Starr AF, Smith DR. Metamaterial electromagnetic cloak at microwave frequencies. *Science (New York, N.Y.)* 2006; **314**(5801):977–980, doi:10.1126/science.1133628.
- [6] Alù A, Engheta N. Achieving transparency with plasmonic and metamaterial coatings. *Physical Review E - Statistical, Nonlinear, and Soft Matter Physics* 2005; **72**(1):1–9, doi:10.1103/PhysRevE.72.016623.
- [7] Monti A, Bilotti F, Toscano A. Optical cloaking of cylindrical objects by using covers made of core-shell nanoparticles. *Optics letters* 2011; **36**(23):4479–4481, doi:10.1364/OL.36.004479.
- [8] Farhat M, Mühlhig S, Rockstuhl C, Lederer F. Scattering cancellation of the magnetic dipole field from macroscopic spheres. *Optics express* 2012; **20**(13):13 896–13 906, doi:10.1364/OE.20.013896.
- [9] Bendsøe MP, Kikuchi N. Generating optimal topologies in structural design using a homogenization method. *Computer Methods in Applied Mechanics and Engineering* 1988; **71**(2):197–224, doi:10.1016/0045-7825(88)90086-2.
- [10] Bendsøe MP. Optimal shape design as a material distribution problem. *Structural Optimization* 1989; **1**(4):193–202, doi:10.1007/BF01650949.
- [11] Andkjær J, Sigmund O. Topology optimized low-contrast all-dielectric optical cloak. *Applied Physics Letters* 2011; **98**(2):021 112, doi:10.1063/1.3540687.
- [12] Andkjær J, Asger Mortensen N, Sigmund O. Towards all-dielectric, polarization-independent optical cloaks. *Applied Physics Letters* 2012; **100**(10):101 106, doi:10.1063/1.3691835.
- [13] Sethian JA, Wiegmann A. Structural Boundary Design via Level Set and Immersed Interface Methods. *Journal of Computational Physics* 2000; **163**(2):489–528, doi:10.1006/jcph.2000.6581.
- [14] Yamada T, Izui K, Nishiwaki S, Takezawa A. A topology optimization method based on the level set method incorporating a fictitious interface energy. *Computer Methods in Applied Mechanics and Engineering* 2010; **199**(45-48):2876–2891, doi:10.1016/j.cma.2010.05.013.
- [15] Choi JS, Yamada T, Izui K, Nishiwaki S, Yoo J. Topology optimization using a reaction-diffusion equation. *Computer Methods in Applied Mechanics and Engineering* 2011; **200**(29-32):2407–2420, doi:10.1016/j.cma.2011.04.013.
- [16] Fujii G, Watanabe H, Yamada T, Ueta T, Mizuno M. Level set based topology optimization for optical cloaks. *Applied physics letters* 2013; **102**(25):251 106.
- [17] Otomori M, Yamada T, Andkjær J, Izui K, Nishiwaki S, Kogiso N. Level Set-Based Topology Optimization for the Design of an Electromagnetic Cloak With Ferrite Material. *IEEE Transactions on Magnetics* 2013; **49**(5):2081–2084, doi:10.1109/TMAG.2013.2239965.
- [18] Isakari H, Nakamoto K, Kitabayashi T, Takahashi T, Matsumoto T. A multi-objective topology optimisation for 2d electro-magnetic wave problems with the level set method and bem. *European Journal of Computational Mechanics* 2016; **25**(1-2):165–193, doi:10.1080/17797179.2016.1181042.
- [19] Jing G, Matsumoto T, Takahashi T, Isakari H, Yamada T. Topology optimization for 2D heat conduction problems using boundary element method and level set method. *Transactions of JASCOME* 2013; **13**(19):91–96.
- [20] Jing G, Isakari H, Matsumoto T, Yamada T, Takahashi T. Level set-based topology optimization for 2D heat conduction problems using BEM with objective function defined on design-dependent boundary with heat transfer boundary condition. *Engineering Analysis with Boundary Elements* 2015; **61**:61–70, doi:10.1016/j.enganabound.2015.06.012.
- [21] Isakari H, Kuriyama K, Harada S, Yamada T, Takahashi T, Matsumoto T. A topology optimisation for three-dimensional acoustics with the level set method and the fast multipole boundary element method. *Mechanical Engineering Journal* 2014; **1**(4):CM0039—CM0039, doi:10.1299/mej.2014cm00.
- [22] Isakari H, Kondo T, Takahashi T, Matsumoto T. A level-set-based topology optimisation for acoustic-elastic coupled problems with a fast bem-fem solver. *to appear in Computer Methods in Applied Mechanics and Engineering* 2016; .
- [23] Greengard L, Rokhlin V. A fast algorithm for particle simulations. *Journal of computational physics* 1987; **73**(2):325–348.
- [24] Rokhlin V. Rapid solution of integral equations of scattering theory in two dimensions. *Journal of Computational Physics* 1990; **86**(2):414–439.
- [25] Hackbusch W. A sparse matrix arithmetic based on h-matrices. part i: Introduction to h-matrices. *Computing* 1999; **62**(2):89–108.
- [26] Hackbusch W, Khoromskij B. A sparse h-matrix arithmetic: general complexity estimates. *Journal of Computational and Applied Mathematics* 2000; **125**(12):479 – 501, doi:http://dx.doi.org/10.1016/S0377-0427(00)00486-6. Numerical Analysis 2000. Vol. VI: Ordinary Differential Equations and Integral Equations.
- [27] Carpio A, Rapun ML. Solving inhomogeneous inverse problems by topological derivative methods. *Inverse Problems* 2008; **24**(4):045 014, doi:10.1088/0266-5611/24/4/045014.
- [28] Chew WC. *Waves and fields in inhomogeneous media*. 1995.
- [29] Bebendorf M. *Hierarchical matrices*. Springer, 2008.